Mühendislik Bilimleri ve Tasarım Dergisi
8(4), 1269 – 1277, 2020
e-ISSN: 1308-6693

Journal of Engineering Sciences and Design
DOI: 10.21923/jesd.816906

Araştırma Makalesi Research Article

GRAPHENE-TUNABLE MID-INFRARED METAMATERIALS BASED ON TITANIUM NITRIDE NANORODS

Erdem ASLAN*, Ekin ASLAN

Department of Electrical and Electronics Engineering, Hatay Mustafa Kemal University, 31060, Hatay, Turkey

Keywords

Plasmonics,
Tunable Metamaterials,
Graphene,
Nanoantenna,
Perfect Absorbers.

Abstract

Graphene-tunable, particle-based and absorber metamaterials are presented which utilize titanium nitride as the plasmonic material. The design of the particle-based nanoantenna array is shown via geometrical parameter sweep simulations. Additionally, the origin of the resonance mode is revealed by decomposing the spectrum into the radiating contributions of multipoles and near-field-enhancement distribution maps. Moreover, the tunability of the designed metamaterial is shown by changing the chemical potential of a monolayer of graphene which is coated on top of the device. To utilize the designed device as an absorber metamaterial, a mirror layer is introduced for the elimination of the transmission through the device. With the aim of obtaining perfect absorption, the thickness values of the functional layers are optimized via parameter sweep simulations. Finally, the tunability of the absorber metamaterial is shown by utilizing a graphene monolayer on top of the nanoantennas and the tuning performance of both architectures are compared. The engineering of graphene-tunable metal-free metamaterials provides a novel strategy for the development of low-cost integrated photonic devices and plasmonic devices which are resistant to high temperatures.

TİTANYUM NİTRİT NANOÇUBUK TABANLI GRAFEN İLE AYARLANABİLİR ORTA-KIZILÖTESİ METAMALZEMELER

Anahtar Kelimeler

Plazmonik,
Ayarlanabilir Metamalzeme,
Grafen,
Nanoanten,
Mükemmel Soğurucu.

Özet

Plazmonik malzeme olarak titanyum nitrit kullanan, grafen ile ayarlanabilir, parçacık ve soğurucu tabanlı metamalzemeler sunulmuştur. Parçacık tabanlı nanoantenin tasarımı, parametre değişimi benzetimleri ile sunulmuştur. Ayrıca, rezonans modlarının kökeni, çok kutuplu modların, tasarlanan yapının tayfına katkılarının belirlenmesi ve yakın alan güçlendirme dağılım haritaları ile ortaya konmuştur. Buna ek olarak, tasarlanan metamalzemenin ayarlanabilirliği, yapının üzerine kaplanmış tek katman grafenin kimyasal potansiyelinin değiştirilmesi ile gösterilmiştir. Tasarlanan cihazın soğurucu metamalzeme olarak kullanılabilmesi amacıyla, yapıdan elektromanyetik geçirgenliği elimine etmek için bir ayna katmanı eklenmiştir. Soğurmanın mükemmel olması için, fonksiyonel yapıların kalınlıkları, parametre değişimi benzetimleri ile optimize edilmiştir. Son olarak, soğurucu yapının ayarlanabilirliği, nanoantenlerin üzerine tek katmanlı grafenin kaplanması ile sağlanmıştır ve parçacık ve soğurucu tabanlı metamalzemelerin ayarlanabilirlik performansları karşılaştırılmıştır. Grafen ile ayarlanabilir, metal kullanılmayan metamalzemelerin mühendisliği, düşük maliyetli tümleşik fotonik cihazların ve yüksek sıcaklıklara dayanıklı plazmonik cihazların geliştirilebilmesi için yeni bir strateji sağlamaktadır.

Alıntı / Cite

Aslan, E., Aslan, E., (2020). Graphene-Tunable Mid-Infrared Metamaterials Based on Titanium Nitride Nanorods, Journal of Engineering Sciences and Design, 8(4), 1269-1277.

* İlgili yazar / Corresponding author: erdem.aslan@mku.edu.tr

Yazar Kimliği / Author ID (ORCID Number)	Makale Süreci / Article Process	
E. Aslan, 0000-0001-6829-9000	**Başvuru Tarihi / Submission Date**	27.10.2020
E. Aslan, 0000-0003-0933-7796	**Kabul Tarihi / Accepted Date**	08.12.2020
	Yayım Tarihi / Published Date	25.12.2020

1. Introduction

Instead of changing the molecular structure and macroscopic geometrical parameters of optical components, electromagnetic metamaterial technology relies on engineering the optical response via altering the subwavelength structure for the realization of optically functional devices (RoyChoudhury et al., 2016; Wenclawiak et al., 2019). As a result, metamaterials have provided a huge degree of freedom to manipulate the electromagnetic waves (Aslan, 2020). Additionally, metamaterials pave the way to access the electromagnetic functionalities which are not observed in nature such as negative refractive index (Pendry, 2000), electromagnetic cloaking (Schurig et al., 2006), inverse Doppler effect (Chen et al., 2011) and optical magnetism (Monticone and Alù, 2014). The preliminary efforts in metamaterial research focused on the development of the devices with fixed spectral response (Shelby et al., 2001; Smith et al., 2000). However, up-to-date research areas require photonic devices with tunable optical properties for the applications such as photonic integrated circuits (Dietrich et al., 2016) and tunable plasmonic sensors (Cen et al., 2018). Hence the tunable metamaterials have attracted significant attention (Hajian et al., 2019; Jiang et al., 2018). There are many techniques to tune the resonant modes of the metamaterials including optical, thermal, mechanical, and electrical controls. Optical tunability relies on the photoconductivity of materials such as silicon (Shen et al., 2009) and gallium arsenide (Zhao et al., 2015). In a similar way, thermally tunable metamaterials exploit the properties of thermal-responsive materials such as vanadium oxide (Bang et al., 2018) and strontium titanate (X. Huang et al., 2019). Additionally, flexible (Liu et al., 2019) and micro-electromechanics metamaterials (Ren et al., 2019) are the examples of the mechanically tunable metamaterials. Electrical control depends on the change of charge carrier concentration by the applied voltage (Fang et al., 2020; Isic et al., 2019; Min et al., 2019). Graphene is one of the most promising materials to be utilized in tunable metamaterials (Zhang et al., 2020; Zou et al., 2019) which is a two-dimensional material composed of hexagonally arranged carbon atoms with an atomic layer thickness. Additionally, graphene can enable the tunability of a metamaterial by the applied external electrostatic voltages (Kim et al., 2012; Xiao et al., 2019; Ye et al., 2019; Y. Zhang et al., 2016).

Surface plasmons are propagating electron density oscillations at the conductor-dielectric interface due to the coupling of the incident light to the conduction electrons of the metal. The non-propagating type of surface plasmons are called localized surface plasmons (LSPs) which is observed on the surface of metallic subwavelength particles (Aslan et al., 2016; Cao et al., 2014). The resonant behavior of LSPs results with the subwavelength confinement of light. Noble metals are the most studied materials to design the LSP resonance (LSPR) based metamaterials however the high ohmic losses of the noble metals restrict the range of plasmonic metamaterial applications (Naik et al., 2013). In the last decade, wide variety of alternative plasmonic materials have been developed such as III-V semiconductors (Zhong et al., 2015), transparent conductive oxides and nitrides (Naik et al., 2011). One of the most promising alternative plasmonic materials is the titanium nitride (TiN) due to its metallic optical properties in visible and longer wavelengths and CMOS fabrication compatibility (Gui et al., 2016). Additionally, TiN is a refractory material hence it can sustain high temperatures which makes it suitable for high-energy-loss applications such as perfect absorbers (Li et al., 2014). Despite the advantages of alternative plasmonic materials, few previous works have focused on the tunable metamaterials which utilize graphene and alternative plasmonic materials (Salemizadeh et al., 2019).

In this study, the design and numerical characterization of tunable particle-based and absorber metamaterials are presented which utilize TiN nanoparticles as plasmonic structures and a graphene layer in order to tune the plasmonic resonances dynamically. First, the particle-based metamaterial is analyzed by revealing the dependence of its reflection spectra to its geometrical parameters. Additionally, the physical origin of the resonant mode is investigated through multipole expansion and field enhancement maps. In order to the tune the plasmonic resonance dynamically, the metamaterial is covered with a monolayer of graphene and the tunability is investigated through the dependence of spectral shift on the electrochemical potential of graphene layer. Moreover, the optical properties and the tunability of the absorber metamaterial is investigated which is derived from the particle-based device by adding a mirror layer. Due to their metal-free design and spectral tunability, the proposed designs can be utilized in tunable optical sensors and integrated photonic devices.

2. Design of the Particle Based Metamaterial

With the aim of designing a metal free and tunable metamaterial, TiN is utilized as the plasmonic material. The designed metamaterial has two significant advantages which are the noble metal-free design and the simple

geometry. The former advantage reduces the ohmic losses which have the highest value at the resonant wavelength and the latter advantage is due to the rod-shape which is an elementary antenna geometry that allows the realization of the metamaterial via low-cost mass-production methods such as nano-stencil fabrication. Fig. 1(a) shows the schematic illustration and the geometrical parameters of the unitcell for the designed metamaterial. The unitcell consists of a 300 nm thick TiN rod shaped nanoantenna as a resonator and a 200 nm thick sapphire (Al_2O_3) substrate. The main geometrical parameters of the nanoantenna are length, L and the width, W. P_x and P_y are the periodicities of the unitcell along the x and y directions, respectively. The dispersion data of TiN is taken from the literature (Bagheri et al., 2015) and the data in the material-database of the Lumerical FDTD Solutions software is used for the sapphire which is taken from the reference (Palik, 1997). During the simulations, the nanoantenna is illuminated from the top-side by a normally-incident plane-wave and the periodic boundary conditions are used along the x and y directions. For the boundaries along the z-axis, perfect match layer is utilized in order to eliminate the reflections. Fig. 1(b) shows the reflectance spectrum of the metamaterial under x-polarized mid-infrared light for several values of L. Light incident on the rod nanoantenna, causes displacement of the conduction band electrons with respect to the central point of the particle which gives rise to a restoring force originating from Coulombic attraction. The electrons that have the oscillation phase with a $\pi/2$ lag according to the electric field of incident light, contributes to the LSPR (Petryayeva and Krull, 2011). The size of the particle along the electric field of the light specify the resonance wavelength hence a redshift of the resonant mode is observed in Fig. 1(b) for the increasing value of the L.

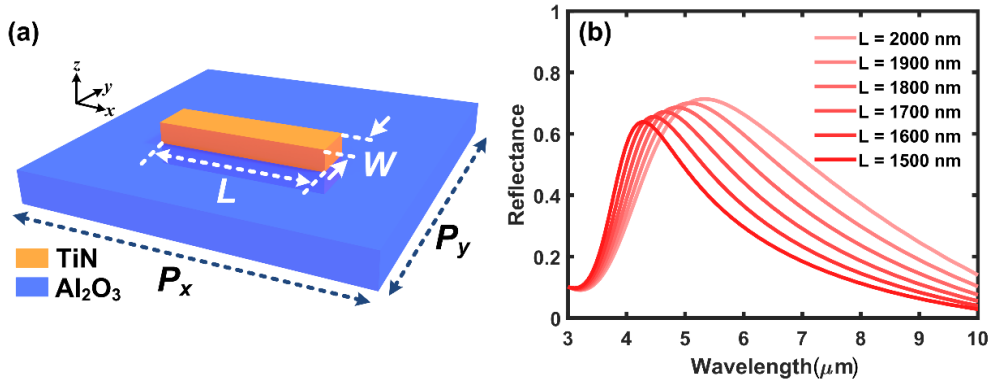

Figure 1. (a) Schematic illustration of the unitcell of the designed particle-based metamaterial. L is the length and W is the width of the nanoantenna. P_x and P_y are the periodicities of the unitcell along the x- and y-axes, respectively. **(b)** Reflectance spectrum of the metamaterial under x-polarized light for various L values while other parameters are kept constant as W = 500 nm, $P_x = P_y$ = 2500 nm.

In order to reveal the physical origin of the resonance mode, the reflectance spectrum for the case of L = 1500 nm is decomposed into the radiating contributions of multipoles by using the localized distribution of the volume current density in the rod antenna (Dong et al., 2013; Y.-W. Huang et al., 2012). Fig. 2(a) shows the scattering power of each moment for the case of L = 1500 nm. In this figure P is the power of dipolar electric moment, M is the dipolar magnetic moment, Tor is the toroidal mode, Q_e is the quadrupolar electric moment and Q_m is the quadrupolar magnetic moment. It is seen in Fig. 2(a) that the resonance mode has a dipolar electric characteristic and this situation is verified by the electric and magnetic field enhancement distribution maps which are shown for the top surface of the nanoantenna in Fig. 2(b) and (c), respectively. Fig 2(b) shows that the electric field enhancement has its maximum value at the corners of the rod antenna which also shows that the locations of highest charge accumulations. Due to the dipolar electric characteristic, a resonant current density occurs which has the maximum value at the edges of the rod antenna and causes a high magnetic-field-enhancement as shown in Fig. 2(c). This situation explains the condition that the magnetic dipole mode is the second dominant mode at the resonant wavelength which is the consequence of the current density.

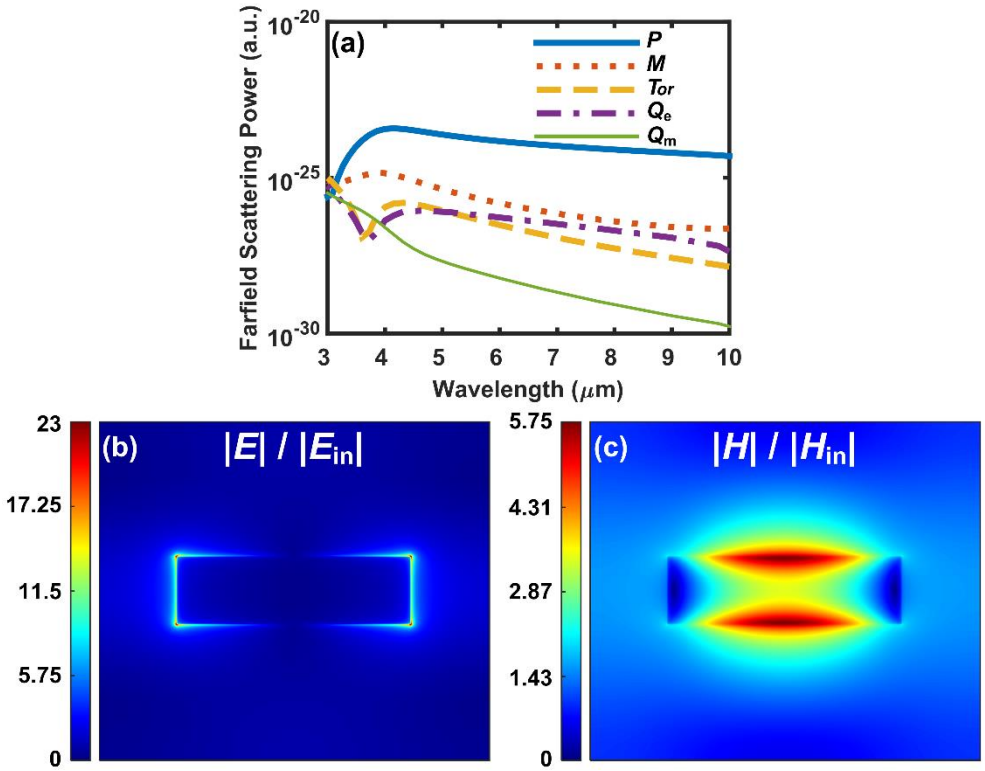

Figure 2. (a) Scattering power of the electromagnetic modes of the reflectance spectra for the case of L = 1500 nm and W = 500 nm. **(b)** Electric field enhancement ($|E|/|E_{in}|$) and **(c)** magnetic field enhancement ($|H|/|H_{in}|$) at the top surface of the nanoantenna for the resonance wavelength of 4272 nm.

3. Tunability of the Particle Based Metamaterial

It is convenient to model the electrical properties of monolayer graphene as surface conductivity σ which is defined by the intraband σ_{intra} and interband σ_{inter} contributions (Andryieuski and Lavrinenko, 2013; Jin et al., 2019).

$$\sigma(\omega) = \sigma_{intra}(\omega) + \sigma_{inter}(\omega) \tag{1}$$

$$\sigma_{intra}(\omega) = \frac{2\kappa_b T e^2}{\pi\hbar^2} \ln\left(2\cosh\frac{E_f}{2\kappa_b T}\right)\frac{i}{(\omega + i\Gamma)} \tag{2}$$

$$\sigma_{inter}(\omega) = \frac{e^2}{4\hbar}\left[H\left(\omega/2\right) + i\frac{4\omega}{\pi}\int_0^\infty \frac{H(\Omega) - H\left(\omega/2\right)}{\omega^2 - 4\Omega^2} d\Omega\right] \tag{3}$$

$$H(\Omega) = \frac{\sinh\left(\hbar\Omega/\kappa_b T\right)}{\left[\cosh\left(\hbar\Omega/\kappa_b T\right) + \cosh\left(E_f/\kappa_b T\right)\right]} \tag{4}$$

In the equations, T is the temperature, E_f is the electrochemical potential, w is the frequency of the incident light and Γ is the inverse of relaxation time. In the THz and the far-infrared region, the intraband contribution is dominant while in the near-infrared and visible frequencies the interband contribution becomes significantly higher (Wang et al., 2019). Monolayer graphene possesses a weak interaction with light hence it has a high optical transparency. The enhanced electromagnetic fields that surrounds the vicinity of plasmonic subwavelength particles can play an intermediate role for the amplification of this interaction via confining the energy of incident light to the graphene layer. Additionally, plasmonic resonances are highly sensitive to the electrical and optical properties of the surrounding environment that an incremental change of the refractive index results with a redshift of the resonant wavelength. Hence the existence of the graphene layer at the electromagnetic hotspot of the nanoantennas can shift the resonance frequency (Low and Avouris, 2014; Nan et al., 2018). Moreover, the E_f value can be controlled by applying an external voltage to the graphene layer which provides the alteration of the surface conductivity of graphene. By utilizing the tunability of the surface conductivity of the graphene, the frequency of the plasmonic resonance of the TiN nanorod antennas can be tuned by changing the applied external voltage.

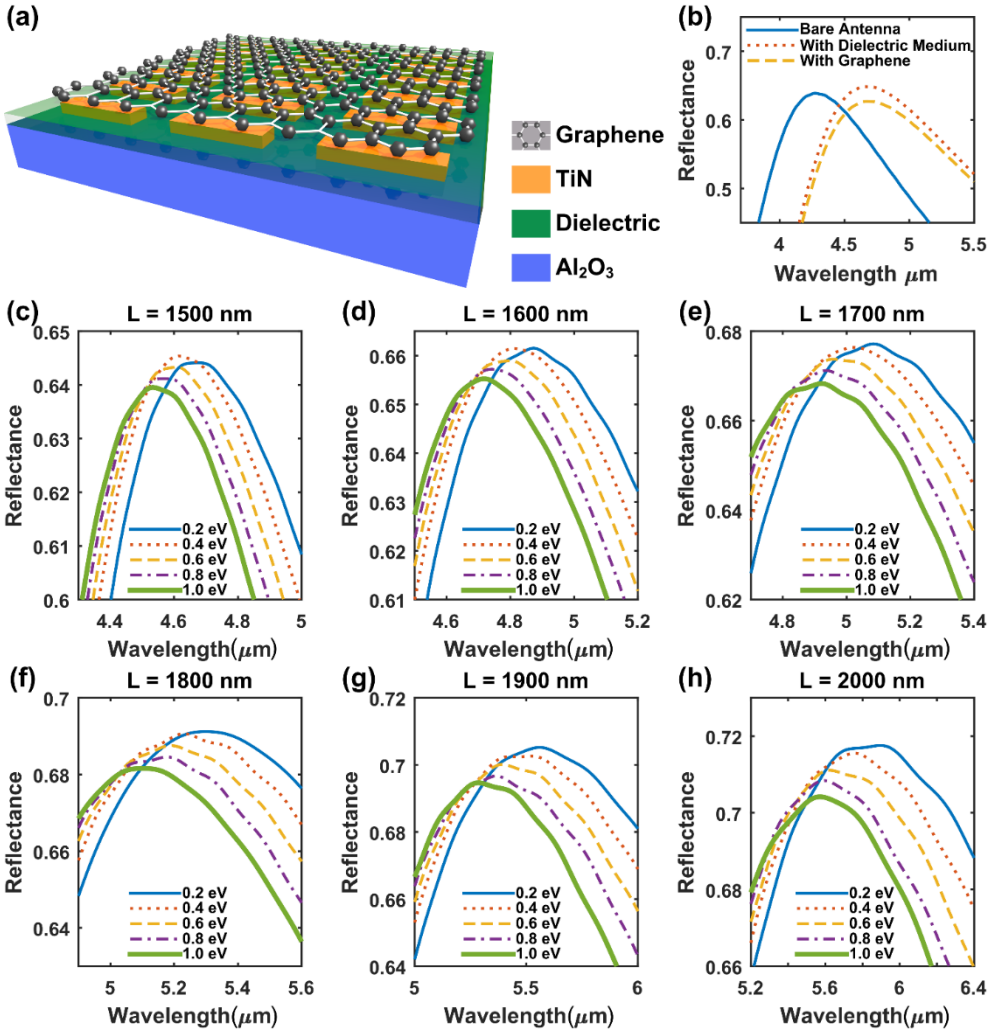

Figure 3. (a) Schematic illustration of the nanoantenna with monolayer graphene on top. **(b)** Reflectance spectra of the bare antenna, antenna with dielectric medium and with graphene on top. Spectra that shows the graphene tuning of the resonance mode for **(c)** L = 1500 nm, **(d)** L = 1600 nm, **(e)** L = 1700 nm, **(f)** L = 1800 nm, **(g)** L = 1900 nm, **(h)** L = 2000 nm.

In order to integrate the graphene layer on top of the designed nanoantenna array, a dielectric layer is utilized that surrounds the nanoantennas and provides a flat surface for coating the graphene layer. The refractive index of the dielectric layer is taken as 1.3 and the thickness of this layer has the same thickness with the TiN nanoantennas as shown in Fig. 3(a). Fig. 3(b) shows the reflectance spectra for the bare nanoantenna array (blue solid line), nanoantenna with dielectric layer (red dotted line) and the antenna array with graphene layer on top (yellow dashed line). Due to the greater refractive index of the dielectric medium, the spectral location of the resonance mode for the dielectric coated antenna array is red-shifted with respect to the resonance wavelength of the bare antenna array. Additionally, it is seen in Fig. 3(b) that the effect of the graphene layer is a slight decrease of the reflectance amplitude which is the result of the absorption of the graphene layer. In order to reveal the effect of the electrochemical potential of the graphene on the plasmonic resonance of TiN rod antennas, simulations for the TiN rod antenna arrays for various L values are ran while sweeping the electrochemical potential of the graphene layer from 0.2 eV to 1 eV. The results of the simulations are presented in Fig. 3 (c)-(h) which also shows the tunability of the dipolar electric resonances.

4. Design of the Absorber Metamaterial

Due to the development in the nanofabrication methods, a wide variety of metamaterial concepts have been developed (Urbas et al., 2016). One of the most remarkable type of these metamaterials are the plasmonic perfect absorbers which have gained great interest due to their near-unity absorption capability and potential applications including the selective thermal emitters (Hossain et al., 2015), spectroscopy (Aslan et al., 2019) and energy conversion (Xie et al., 2014). With the aim of designing a tunable absorber metamaterial, the structure is modified as shown in Fig. 1(a) by adding a TiN mirror layer under the sapphire layer. The schematic illustration of the absorber metamaterial is shown in Fig 4(a). In this configuration the main principle of absorption is minimizing the reflectance by impedance matching through the nanoantennas and the elimination of transmission

by the TiN film which electromagnetically couples to the top TiN nanoantennas. This coupling is supported by the sapphire spacer layer. In our simulations, the structure is top illuminated by a *x*-polarized normally-incident plane wave and the obtained spectra is shown in Fig. 4(b) for L = 1500 nm, W = 500 nm, P_x = P_y = 2500 nm and the thickness of antennas and the spacer layer are 300 nm and 500 nm, respectively. It is seen that the transmission is zero hence the absorbance (*Abs*) can be calculated from the reflectance (*Ref*) data as *Abs* = 1 – *Ref*. For the designed structure, the incident light is coupled to the top antenna which results with dipolar charge distribution and this distribution is mirrored by the bottom TiN film via electromagnetic coupling. The ohmic losses arising from the conduction current is the main dissipation mechanism for the energy of incident light.

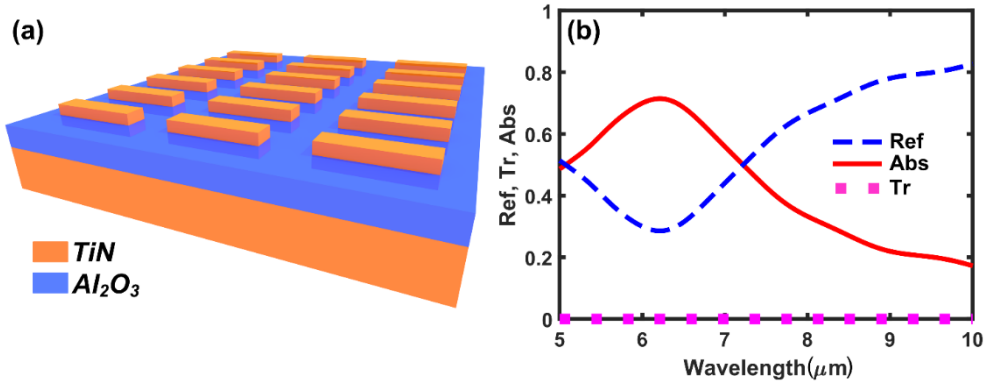

Figure 4. (a) Schematic illustration of the unitcell of the absorber metamaterial. **(b)** Reflectance, absorbance, and transmittance spectrum of the absorber under *x*-polarized light for L = 1500 nm, W = 500 nm, P_x = P_y = 2500 nm.

To maximize the absorption performance of the metamaterial, the thickness values of the antenna ($t_{Antenna}$) and the spacer layer (t_{Spacer}) must be optimized which are schematically illustrated in Fig 5(a). For this purpose, thickness sweep simulation results are shown in Fig. 5(b). The thickness values of the nanoantenna and the spacer layer are changed from 50 nm up to 500 nm with a step of 50 nm while other geometrical parameters are kept constant as L = 1500 nm, W = 500 nm and P_x = P_y = 2500 nm. It is observed in Fig. 5(b) that there is a region at which near-perfect absorption can be obtained and, in this region, $t_{Antenna}$ and t_{Spacer} is inversely proportional. Hence, it is preferred to keep the antenna thinner than the spacer layer and the preferred thickness values are $t_{Antenna}$ = 100 nm and t_{Spacer} = 300 nm. Fig 5(c) shows the dependence of the absorption spectrum on the L parameter for the optimized thickness parameters while other geometrical parameters are fixed. It is observed that increasing the value of L parameter results with a red-shift of the resonant mode while maintaining the near-perfect-absorption at the resonance wavelength.

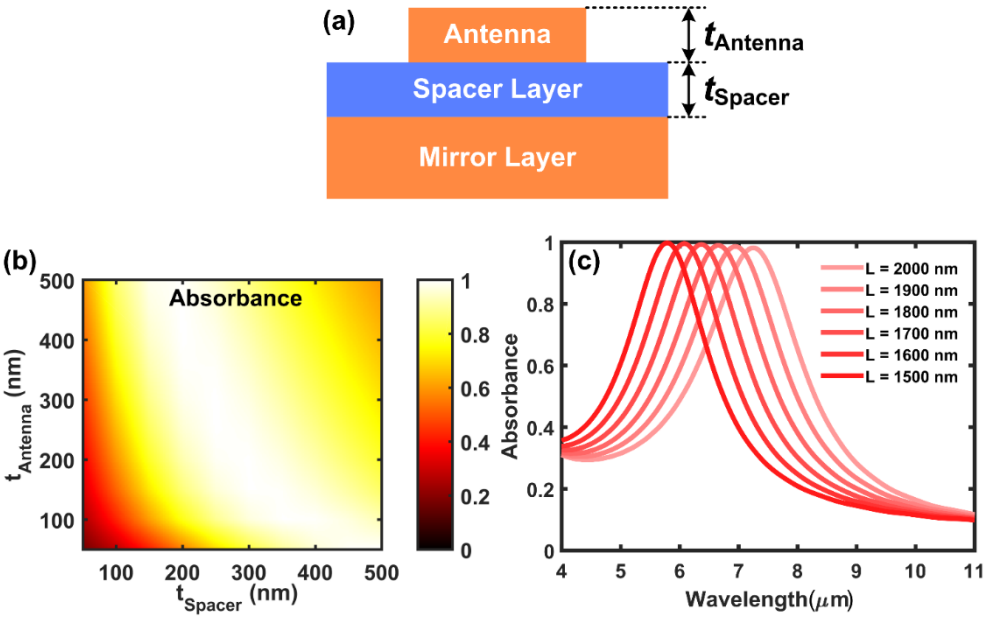

Figure 5. (a) Schematic illustration of the cross-sectional view of the absorber metamaterial which shows the layer thickness parameters. **(b)** Dependence of the absorbance on the thickness of the antenna and the spacer layer. **(c)** Absorbance results of L-sweep with the optimized thickness values.

5. Tunability of the Absorber Metamaterial

In order to make the absorber tunable, a dielectric layer is utilized that has the same thickness of the TiN antennas to support the top graphene layer as shown in Fig. 6(a) which is the same strategy for the particle-based device. During the simulations, the chemical potential of the graphene layer is swept from 0.2 eV to 1 eV with a step of 0.2 eV for various values of L and the results are presented in Fig. 6(b)-(g). For all the situations in Fig6(b)-(g), a blue-shift is observed for the increasing value of the electrochemical potential of the graphene layer. This situation can be explained by the increased number of the free electrons and the transfer of these electrons to the nanoantennas where they contribute to the LSP oscillations (Nan et al., 2018). In order to quantify and compare the tuning performance of the particle-based and absorber metamaterials, the amount of resonance-wavelength shift is calculated which is defined as the difference between the resonance wavelengths for the cases of E_f = 0.2 eV and E_f = 1 eV. The results are summarized in Table 1 for various values of the L parameter and it is observed that the resonance-wavelength-shift increases for the increasing value of the L parameter for both device architectures. However, the resonance-wavelength-shift is much higher for the absorber device than the particle-based device. This situation can be attributed to the higher field-enhancement of the absorber device which is calculated as 37 at its maximum. The highest resonance-wavelength-shift is obtained as 570 nm for the absorber device with a L value of 2000 nm.

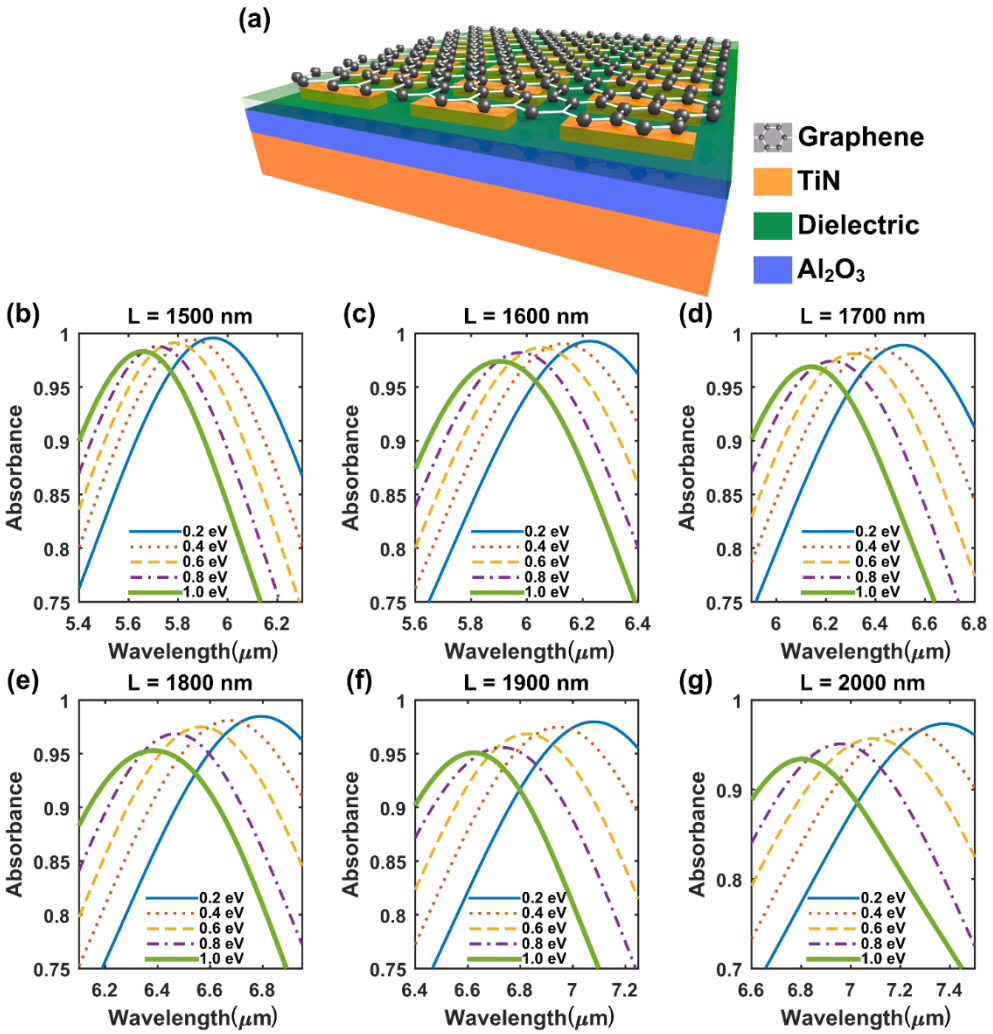

Figure 6. (a) Schematic illustration of the absorber with monolayer graphene on top. Spectra that shows the graphene tuning of the absorbance mode for **(b)** L = 1500 nm, **(c)** L = 1600 nm, **(d)** L = 1700 nm, **(e)** L = 1800 nm, **(f)** L = 1900 nm, **(g)** L = 2000 nm.

Table 1. Amount of resonance-wavelength-shift while the electrochemical potential of graphene is increased from 0.2 eV to 1 eV for the particle-based ($\Delta\lambda_{particle}$) and absorber $\Delta\lambda_{absorber}$) metamaterials which have various values of L parameter.

	***L* value**					
	1500 nm	**1600 nm**	**1700 nm**	**1800 nm**	**1900 nm**	**2000 nm**
$\Delta\lambda_{particle}$	160 nm	150 nm	160 nm	200 nm	280 nm	330 nm
$\Delta\lambda_{absorber}$	290 nm	330 nm	370 nm	410 nm	450 nm	570 nm

6. Conclusions

The design and numerical demonstration of graphene-tunable TiN-based metamaterials have been presented. The designed metamaterials were based on the particle and absorber architectures. The design of the particle-based nanoantenna array has been demonstrated via geometrical parameter sweep simulations. Additionally, the origin of the resonance mode has been revealed by decomposing the spectrum into the radiating contributions of multipoles and near-field-enhancement distribution maps. Moreover, the tunability of the designed metamaterial has been shown by changing the chemical potential of a monolayer of graphene which was coated on top of the device. To utilize the designed device as an absorber metamaterial, a mirror layer has been introduced for the elimination of the transmission through the device. With the aim of obtaining perfect absorption, the thicknesses of the TiN nanoantennas and the sapphire spacer layer have been optimized via parameter sweep simulations. Finally, the tunability of the absorber metamaterial has been shown by utilizing a graphene monolayer on top of the TiN nanoantennas and compared the amount of resonance-wavelength-shift values of both architectures. The engineering of graphene-tunable TiN-based metamaterials provides a novel strategy for the development of low-cost integrated photonic devices and plasmonic devices which are resistant to high temperatures.

Acknowledgement

The work described in this paper is supported by Scientific Research Projects Coordination Center of Hatay Mustafa Kemal University (Project ID: 19.M.016).

Conflict of Interest

No conflict of interest was declared by the authors.

References

Andryieuski, A., Lavrinenko, A. V., 2013. Graphene Metamaterials Based Tunable Terahertz Absorber: Effective Surface Conductivity Approach. Optics Express, 21(7), 9144.

Aslan, E., 2020. Conformal Talbot-Effect-Focusing Performance of Nested Gallium-Doped Zinc Oxide Nanorings at Communication Wavelength. Photonics and Nanostructures - Fundamentals and Applications, 42, 100839.

Aslan, E., Aslan, E., Wang, R., Hong, M. K., Erramilli, S., Turkmen, M., Saracoglu, O. G., Dal Negro, L., 2016. Multispectral Cesaro-Type Fractal Plasmonic Nanoantennas. ACS Photonics, 3(11), 2102–2111.

Aslan, E., Aslan, E., Saracoglu, O. G., Turkmen, M., 2019. An Effective Triple-Band Enhanced-Infrared-Absorption Detection by Honeycomb-Shaped Metamaterial-Plasmonic Absorber. Sensors and Actuators A: Physical, 288, 149–155.

Bagheri, S., Zgrabik, C. M., Gissibl, T., Tittl, A., Sterl, F., Walter, R., De Zuani, S., Berrier, A., Stauden, T., Richter, G., Hu, E. L., Giessen, H., 2015. Large-Area Fabrication of TiN Nanoantenna Arrays for Refractory Plasmonics in the Mid-Infrared by Femtosecond Direct Laser Writing and Interference Lithography [Invited]. Optical Materials Express, 5(11), 2625–2633.

Bang, S., Kim, J., Yoon, G., Tanaka, T., Rho, J., 2018. Recent Advances in Tunable and Reconfigurable Metamaterials. Micromachines, 9(11), 560.

Cao, J., Sun, T., Grattan, K. T. V., 2014. Gold Nanorod-Based Localized Surface Plasmon Resonance Biosensors: A Review. Sensors and Actuators B: Chemical, 195, 332–351.

Cen, C., Lin, H., Huang, J., Liang, C., Chen, X., Tang, Y., Yi, Z., Ye, X., Liu, J., Yi, Y., Xiao, S., 2018. A Tunable Plasmonic Refractive Index Sensor with Nanoring-Strip Graphene Arrays. Sensors, 18(12), 4489.

Chen, J., Wang, Y., Jia, B., Geng, T., Li, X., Feng, L., Qian, W., Liang, B., Zhang, X., Gu, M., Zhuang, S., 2011. Observation of the Inverse Doppler Effect in Negative-Index Materials at Optical Frequencies. Nature Photonics, 5, 239–242.

Dietrich, C. P., Fiore, A., Thompson, M. G., Kamp, M., Höfling, S., 2016. GaAs Integrated Quantum Photonics: Towards Compact and Multi-Functional Quantum Photonic Integrated Circuits. Laser and Photonics Reviews, 10(6), 870–894.

Dong, Z. G., Zhu, J., Yin, X., Li, J., Lu, C., Zhang, X.,2013. All-Optical Hall Effect by the Dynamic Toroidal Moment in A Cavity-Based Metamaterial. Physical Review B - Condensed Matter and Materials Physics, 87(24), 245429.

Fang, J., Huang, J., Gou, Y., Shang, Y., 2020. Research on Broadband Tunable Metamaterial Absorber Based on PIN Diode. Optik, 200, 163171.

Gui, L., Bagheri, S., Strohfeldt, N., Hentschel, M., Zgrabik, C. M., Metzger, B., Linnenbank, H., Hu, E. L., Giessen, H., 2016. Nonlinear Refractory Plasmonics with Titanium Nitride Nanoantennas. Nano Letters, 16(9), 5708–5713.

Hajian, H., Ghobadi, A., Butun, B., Ozbay, E., 2019. Active Metamaterial Nearly Perfect Light Absorbers: A Review [Invited]. Journal of the Optical Society of America B, 36(8), F131–F143.

Hossain, M. M., Jia, B., Gu, M., 2015. A Metamaterial Emitter for Highly Efficient Radiative Cooling. Advanced Optical Materials, 3(8), 1047–1051.

Huang, X., He, W., Yang, F., Ran, J., Yang, Q., Xie, S., 2019. Thermally Tunable Metamaterial Absorber Based on Strontium Titanate in the Terahertz Regime. Optical Materials Express, 9(3), 1377.

Huang, Y.-W., Chen, W. T., Wu, P. C., Fedotov, V., Savinov, V., Ho, Y. Z., Chau, Y.-F., Zheludev, N. I., Tsai, D. P., 2012. Design of Plasmonic Toroidal Metamaterials at Optical Frequencies. Optics Express, 20(2), 1760–1768.

Isic, G., Sinatkas, G., Zografopoulos, D. C., Vasic, B., Ferraro, A., Beccherelli, R., Kriezis, E. E., Belic, M., 2019. Electrically Tunable Metal-Semiconductor-Metal Terahertz Metasurface Modulators. IEEE Journal of Selected Topics in Quantum Electronics, 25(3), 8500108.

Jiang, N., Zhuo, X., Wang, J., 2018. Active Plasmonics: Principles, Structures, and Applications. Chemical Reviews, 118(6), 3054–3099.

Jin, X., Wang, F., Huang, S., Xie, Z., Li, L., Han, X., Chen, H., Zhou, H., 2019. Coherent Perfect Absorber with Independently Tunable Frequency Based on Multilayer Graphene. Optics Communications, 446, 44–50.

Kim, J., Son, H., Cho, D. J., Geng, B., Regan, W., Shi, S., Kim, K., Zettl, A., Shen, Y.R., Wang, F., 2012. Electrical Control of Optical Plasmon Resonance with Graphene. Nano Letters, 12(11), 5598–5602.

Li, W., Guler, U., Kinsey, N., Naik, G. V., Boltasseva, A., Guan, J., Shalaev, V. M.,Kildishev, A. V., 2014. Refractory Plasmonics with Titanium Nitride: Broadband Metamaterial Absorber. Advanced Materials, 26(47), 7959–7965.

Liu, C., Cai, J., Li, X., Zhang, W., Zhang, D., 2019. Flexible and Tunable Electromagnetic Meta-Atom Based on Silver Nanowire Networks. Materials and Design, 181, 107982.

Low, T., Avouris, P., 2014. Graphene Plasmonics for Terahertz to Mid-Infrared Applications. ACS Nano, 8(2), 1086–1101.

Min, L., Wang, W., Huang, L., Ling, Y., Liu, T., Liu, J., Luo, C., Zeng, Q., 2019. Direct-Tuning Methods for Semiconductor Metamaterials. Scientific Reports, 9, 17622.

Monticone, F., Alù, A., 2014. The Quest for Optical Magnetism: From Split-Ring Resonators to Plasmonic Nanoparticles and Nanoclusters. Journal of Materials Chemistry C, 2, 9059–9072.

Naik, G. V., Kim, J., Boltasseva, A., 2011. Oxides and Nitrides as Alternative Plasmonic Materials in the Optical Range [Invited]. Optical Materials Express, 1(6), 1090–1099.

Naik, G. V., Shalaev, V. M., Boltasseva, A., 2013. Alternative Plasmonic Materials: Beyond Gold and Silver. Advanced Materials, 25(24), 3264–3294.

Nan, H., Chen, Z., Jiang, J., Li, J., Zhao, W., Ni, Z., Gu, X., Xiao, S., 2018. The Effect of Graphene on Surface Plasmon Resonance of Metal Nanoparticles. Physical Chemistry Chemical Physics, 20(38), 25078–25084.

Palik, E. D., 1997. Handbook of Optical Constants of Solids. Handbook of Optical Constants of Solids (Vol. I–III), College Park, Maryland, Academic Press.

Pendry, J. B., 2000. Negative Refraction Makes a Perfect Lens. Physical Review Letters, 85(18), 3966–3969.

Petryayeva, E., Krull, U. J., 2011. Localized Surface Plasmon Resonance: Nanostructures, Bioassays and Biosensing-A Review. Analytica Chimica Acta, 706(1), 8–24.

Ren, Z., Chang, Y., Ma, Y., Shih, K., Dong, B., Lee, C., 2019. Leveraging of MEMS Technologies for Optical Metamaterials Applications. Advanced Optical Materials, 1900653.

RoyChoudhury, S., Rawat, V., Jalal, A. H., Kale, S. N., Bhansali, S., 2016. Recent Advances in Metamaterial Split-Ring-Resonator Circuits as Biosensors and Therapeutic Agents. Biosensors and Bioelectronics, 86, 595–608.

Salemizadeh, M., Mahani, F. F., Mokhtari, A., 2019. Tunable Mid-Infrared Graphene-Titanium Nitride Plasmonic Absorber for Chemical Sensing Applications. Journal of the Optical Society of America B, 36(10), 2863–2870.

Schurig, D., Mock, J. J., Justice, B. J., Cummer, S. A., Pendry, J. B., Starr, A. F., Smith, D. R., 2006. Metamaterial Electromagnetic Cloak at Microwave Frequencies. Science, 314(5801), 977–980.

Shelby, R. A., Smith, D. R., Schultz, S., 2001. Experimental Verification of a Negative Index of Refraction. Science, 292(5514), 77–79.

Shen, N.-H., Kafesaki, M., Koschny, T., Zhang, L., Economou, E. N., Soukoulis, C. M., 2009. Broadband Blueshift Tunable Metamaterials and Dual-Band Switches. Physical Review B - Condensed Matter and Materials Physics, 79(16), 161102.

Smith, D. R., Padilla, W. J., Vier, D. C., Nemat-Nasser, S. C., Schultz, S., 2000. Composite Medium with Simultaneously Negative Permeability and Permittivity. Physical Review Letters, 84(18), 4184–4187.

Urbas, A. M. et al., 2016. Roadmap on Optical Metamaterials. Journal of Optics, 18(9), 093005.

Wang, R., Ren, X.-G., Yan, Z., Jiang, L. J., Sha, W. E. I., Shan, G.-C., 2019. Graphene Based Functional Devices: A Short Review. Frontiers of Physics, 14(1), 13603.

Wenclawiak, M., Kainz, M. A., Unterrainer, K., Darmo, J., 2019. Dielectric Control of Localized Plasmons in Terahertz Metamaterials. Photonics and Nanostructures - Fundamentals and Applications, 37, 100734.

Xiao, D., Liu, Q., Lei, L., Sun, Y., Ouyang, Z., Tao, K., 2019. Coupled Resonance Enhanced Modulation for a Graphene-Loaded Metamaterial Absorber. Nanoscale Research Letters, 14, 32.

Xie, Y., Fan, X., Wilson, J. D., Simons, R. N., Chen, Y., Xiao, J. Q., 2014. A Universal Electromagnetic Energy Conversion Adapter Based on a Metamaterial Absorber. Scientific Reports, 4(1), 6301.

Ye, L., Zeng, F., Zhang, Y., Liu, Q. H., 2019. Composite Graphene-Metal Microstructures for Enhanced Multiband Absorption Covering the Entire Terahertz Range. Carbon, 148, 317–325.

Zhang, J., Wei, X., Rukhlenko, I. D., Chen, H.-T., Zhu, W., 2020. Electrically Tunable Metasurface with Independent Frequency and Amplitude Modulations. ACS Photonics, 7(1), 265–271.

Zhang, Y., Li, T., Chen, Q., Zhang, H., O'Hara, J. F., Abele, E., Taylor, J., Chen, H.T., Azad, A. K., 2016. Independently Tunable Dual-Band Perfect Absorber Based on Graphene at Mid-Infrared Frequencies. Scientific Reports, 5, 18463.

Zhao, X., Fan, K., Zhang, J., Seren, H. R., Metcalfe, G. D., Wraback, M., Averitt, R.D., Zhang, X., 2015. Optically Tunable Metamaterial Perfect Absorber on Highly Flexible Substrate. Sensors and Actuators, A: Physical, 231, 74–80.

Zhong, Y., Malagari, S. D., Hamilton, T., Wasserman, D., 2015. Review of Mid-Infrared Plasmonic Materials. Journal of Nanophotonics, 9(1), 093791.

Zou, Y., Cao, J., Gong, X., Qian, R., An, Z., 2019. Ultrathin and Electrically Tunable Metamaterial with Nearly Perfect Absorption in Mid-Infrared. Applied Sciences, 9(16), 3358.